

Microstructure analysis of a SmCo/Fe exchange spring bilayer

Yuzi Liu,^{1,2,3} Y. Q. Wu,¹ M. J. Kramer,^{1,a)} Y. Choi,^{2,4} J. S. Jiang,⁴ Z. L. Wang,³ and J. P. Liu²

¹Materials and Engineering Physics Program, Ames Laboratory of USDOE, Ames, Iowa 50011, USA

²Department of Physics, University of Texas at Arlington, Arlington, Texas 76019, USA

³School of Materials Science and Engineering, Georgia Institute of Technology, Atlanta, Georgia 30332 USA

⁴Materials Science Division, Argonne National Laboratory, Argonne, Illinois 60439 USA

(Received 23 June 2008; accepted 16 August 2008; published online 10 November 2008)

The microstructure of a magnetron sputtered Cr(20 nm)/Sm–Co(20 nm)/Fe(20 nm)/Cr(5 nm) exchange spring magnet was studied using an advanced analytical transmission electron microscopy to better understand the relationship between its chemistry and structure to enhance the energy product. It is shown that the Fe atoms diffuse into the well textured Sm–Co layer, causing a transition from the stoichiometric Sm₂Co₇ near the Sm–Co/Cr interface to a defected Sm(Co,Fe)₅ in the Sm–Co–Fe intermixed area. The graded intermixed layer between Sm–Co and pure Fe gives rise to a compositionally enhanced energy product. © 2008 American Institute of Physics.

[DOI: 10.1063/1.2978325]

The energy product of permanent magnets can be considerably increased by judicious mixing of nanoscaled hard and soft magnetic phases.¹ There are many ways to produce these nanocomposite magnets: rapid solidification,² chemical self-assembly,³ and mechanical ball milling.⁴ While these bulk methods have made some strides in increasing the energy product over conventional processing, the results are far from their theoretical maximum.⁵ Complex microstructures in bulk nanocomposites complicate the unraveling contributions from individual features, including length scales of the hard and soft magnetic phases, orientation relationships, and chemical composition, which are most effective in improving the exchange coupling. Thin film techniques, such as magnetron sputtering, can produce artificial multilayers with specific orientations and compositions to better study the mechanisms of exchange coupling;^{6–8} in particular, a chemically graded interface of a magnetically hard-soft material can improve the energy product.⁹ Recently, it was found that the Fe diffusion into a Sm–Co layer resulted in an intermixed layer which leads to an enhanced exchange coupling.^{8,10} In this letter, we will discuss the chemistry of the phases near the interface and their orientation relationships that induce this enhancement.

A JEOL 4000EX and a FEI Tecnai G² F20 scanning transmission electron microscope (STEM) were employed to study the microstructure of a Sm–Co/Fe bilayer within a Cr(20 nm)/Sm–Co(20 nm)/Fe(20 nm)/Cr(5 nm) multilayer fabricated using magnetron sputtering.^{6,9} The epitaxial Sm–Co layer with a nominal composition of Sm₂Co₇ was deposited at 400 °C on a 20 nm Cr(211) buffer layer on a single crystal MgO substrate followed by an Fe overlayer. Instead of postdeposition annealing as was done in Ref. 9, the Fe layer in this study was deposited at 400 °C. This high temperature deposition also created a diffused interface and led to an increased nucleation field.⁸ Cross-sectional transmission electron microscopy (TEM) specimens were pre-

pared by the “sandwich” method in two orientations, along and orthogonal to the in-plane magnetic hard axis.

A bright field TEM image shows the entire sequence of the Cr, Sm–Co, and Fe layers on the MgO substrate [Fig. 1(a)]. The selected area electron diffraction (SAED) pattern covering all layers including the MgO matrix provides the crystallographic details [Fig. 1(b)]. While the diffraction patterns from the Cr and Fe layers are overlapped, the SAED pattern can be indexed to obtain the following crystalline orientation relationships: $[100]_{\text{MgO}} \parallel [001]_{\text{SmCo}} \parallel [-110]_{\text{Fe\&Cr}}$, $[01-1]_{\text{MgO}} \parallel [-110]_{\text{SmCo}} \parallel [110]_{\text{Fe\&Cr}}$, and $[0-1-1]_{\text{MgO}} \parallel [-1-10]_{\text{SmCo}} \parallel [002]_{\text{Fe\&Cr}}$.

Line scan energy dispersive x-ray spectroscopy (EDS) performed in STEM mode was used to investigate the elemental distribution across the layers with an electron probe size of ~ 2 nm. High angle annular dark field (HAADF)

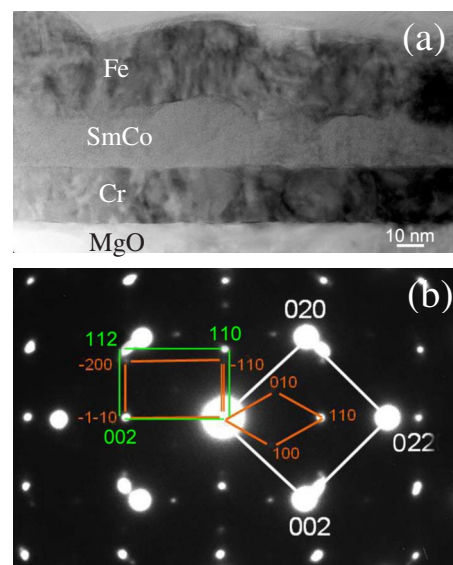


FIG. 1. (Color online) (a) The bright field image and (b) corresponding SAED pattern of Cr(20 nm)/Sm–Co(20 nm)/Fe(20 nm)/Cr(5 nm). Orange lines: SmCo reflections for the [001]; green lines: Fe/Cr [-110]; white lines: MgO [100] zone axes.

^{a)}Electronic mail: mjramer@ameslab.gov.

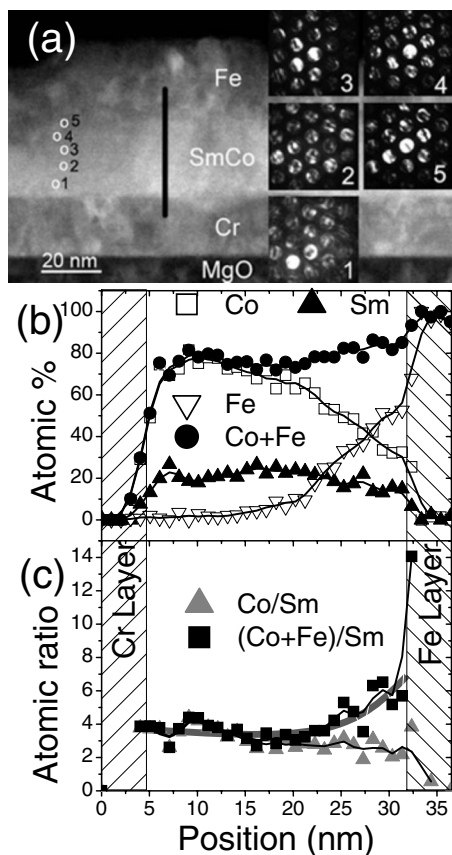


FIG. 2. (a) is the HAADF image with five CBED patterns corresponding to five different areas marked with 1–5. (b) The quantified line scan EDS along the strong black line in (a). (c) The Co/Sm and (Co+Fe)/Sm ratio. The wide black belt is a guide for the eye.

image of the multilayers and the corresponding convergent beam electron diffraction (CBED) patterns taken from the Sm–Co layer are shown in Fig. 2(a). The HAADF is brighter in the nominal Sm–Co layer due to its higher average atomic mass compared to those of the other layers. The insets showing the CBED patterns demonstrate that the crystal structure is well aligned and nominally hexagonal across the thickness of the Sm–Co layer. The elemental concentration along the film's cross section is shown in Fig. 2(b). Both the HAADF and the elemental analysis across the Cr/Sm–Co indicate a sharp interface both chemically and structurally. On the other hand, the Sm–Co/Fe interface is not as sharp in the HAADF image as the Cr/Sm–Co layer, indicative of a closer similarity in average atomic mass across this interface.¹¹ This is consistent with the EDS line scan. While we note that the SmCo and Fe surface shows some roughness [Figs. 1(a) and 2(a)], similar samples with less interfacial mixing and similar overall roughness had smaller energy products (BH_{\max}).⁹ The enhancement in BH_{\max} is attributed to the increased nucleation field energy product over the entire sample and as such, unrelated to the surface roughness. The Sm–Co layer spans from ~ 5 to 32 nm, as indicated in Fig. 2(b). The Sm concentration is nearly constant over the lower half of this region, 20 ± 3 at. %, and shows a small decrease along the upper half. On the contrary, the percentage of Co decreases from 75 ± 3 at. % in the lower half of the Sm–Co layer to 25 at. % close to the upper interface. Based on both electron diffraction and EDS analysis, the lower region of the Sm–Co layer is the hexagonal Sm_2Co_7 (Ce_2Ni_7 type, $P6_3/mmc$,

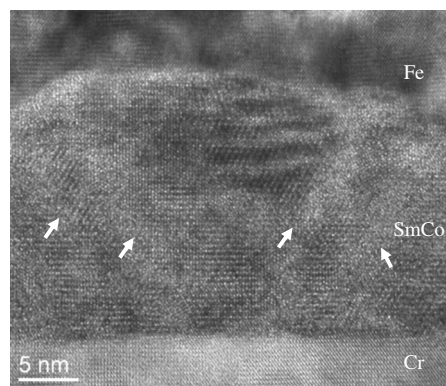


FIG. 3. The HREM image of the multilayers. The lower regions of the Sm:Co layer shown are nearly epitaxial on Cr. The middle to upper parts of the Sm–Co layer shows many boundaries as indicated by the white arrows.

$a=5.045$ Å, $c=24.317$ Å).¹² The concentration of Fe increases slowly from ~ 0 at. % near the middle of the Sm–Co layer to 67 ± 3 at. % at the Sm–Co/Fe interface. The combined Co and Fe total concentration increases from 75 ± 3 to 83 ± 3 at. % close to the upper interface. The (Co, Fe)/Sm atomic ratio increases from about 7:2 in the lower half of the SmCo layer to about 5:1 close to the Fe layer as in Fig. 2(c). These results were repeated on five different crystal structures of Sm_2Co_7 and SmCo_5 (CaCu_5 type, $P6/mmm$ $a=4.997$ Å, $c=3.978$ Å), it is difficult to differentiate the two phases from electron diffraction patterns [Fig. 1(b) and inserted CBED patterns in Fig. 2(a)] when imaging along the [001] axes. In order to determine the details of the Sm–Co/Fe microstructure, high resolution electron microscopy (HREM) images were obtained from the parallel (Fig. 3) and orthogonal directions [Fig. 4(d)]. The SmCo layer is well textured but shows high density grain boundaries through the middle of the Sm–Co layer, as marked by white arrows in Fig. 3. These boundaries are potentially high effective diffusion networks for Fe. Many of the Sm–Co(Fe) compounds have similar subcell structures. For instance, the Sm_2Co_7 and SmCo_5 are composed of similar stacking of Sm–Co and Co layers along the c axis. The symmetry of the simpler 2:7 crystal structure is disrupted by an additional Sm layer which is offset by an $a^{1/2}$ unit cell in the ab plane from the normal

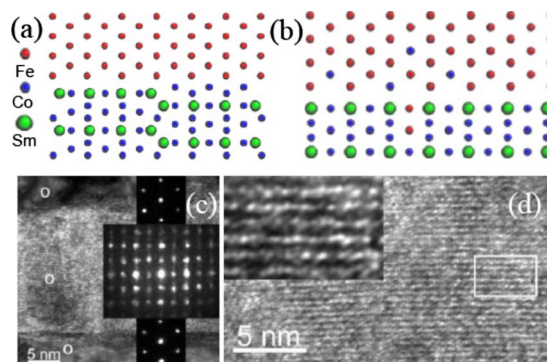


FIG. 4. (Color online) (a) The atomic schematic of Sm_2Co_7 and Fe. Fe will diffuse by the Co channel into Sm_2Co_7 to form $\text{Sm}(\text{Co},\text{Fe})_5$ as shown in (b) after atom arrangement. (c) The CBED patterns from Cr, SmCoFe mixed, and Fe layers from a sample orthogonal to that shown in previous figures. (d) HREM image showing numerous planar defects. The top-left inset is the magnification of the profiled area in this image.

stacking along the c axis, giving rise to a unit cell which is nearly six times the 1:5 compound [Figs. 4(a) and 4(b)].¹² Since small amounts of Fe intermix readily with Sm–Co to form Sm–Co–Fe and that the SmCo₅ phase will form in the Co rich area,¹³ it is expected that a Sm(Co,Fe)₅ phase would form in the Co and Fe rich areas. The chemical and structural analyses suggest that Fe atoms diffuse through the grain boundaries first, then intercalate into Sm₂Co₇ along the channels of pure Co planes, changing the stoichiometry from 2:7 to Sm/(Co, Fe) 1:5. The large degree of diffuse scattering in the Sm–Co(Fe) layer is in accord with this model. Figure 4(a) shows the simulated crystal structures of [111] Fe and the [100] Sm₂Co₇ and their epitaxial relationship, while the same orientation is shown for Sm(Co,Fe)₅ and Fe [Fig. 4(b)]. The $a^{1/2}$ unit cell shift in the double Sm layer in the 2:7 and its absence in the 1:5 compound can be easily seen in this schematic. The orientation relationships for this projection are confirmed by CBED patterns [Fig. 4(c)] while the defected unit cell can be seen in the HREM of Fig. 4(d). These features are all consistent with the SmCo phase transforming from Sm₂Co₇ near the Sm–Co/Cr interface to Sm(Co,Fe)₅ due to downward diffusion of Fe into the Sm–Co layer. This gives rise to an intermixed layer of Sm(Co,Fe)₅ between Sm₂Co₇ and pure Fe layers.

As was demonstrated by Guo *et al.*,¹⁴ a compositionally graded layer will result in an increase in the effective exchange coupling compared to a sharp interface between the hard and soft phases. We show here that the diffusion of Fe into the nominal Sm₂Co₇ compound from the Fe overlayer results in a defected Sm(Co,Fe)₅ intermixed region, giving rise to an exchange enhancement in this sample. It is helpful to explain the role of the chemical graded structure in energy product enhancing.

This work is supported by ONR/MURI under Grant No. N00014-05-1-0497. Work at Ames Laboratory was supported by the U.S. Department of Energy, Office of Science, under Contract No. DE-AC02-07CH11358.

- ¹D. J. Sellmyer, *Nature (London)* **420**, 374 (2002).
- ²J. Bauer, M. Seeger, A. Zern, and H. Kronmuller, *J. Appl. Phys.* **80**, 1667 (1996).
- ³H. Zeng, J. Li, J. P. Liu, Z. L. Wang, and S. H. Sun, *Nature (London)* **420**, 395 (2002).
- ⁴V. M. Chakka, B. Altuncevahir, Z. Q. Jin, Y. Li, and J. P. Liu, *J. Appl. Phys.* **99**, 08E912 (2006).
- ⁵R. Skomski and J. M. D. Coey, *Phys. Rev. B* **48**, 15812 (1993).
- ⁶E. E. Fullerton, J. S. Jiang, M. Grimsditch, C. H. Sowers, and S. D. Bader, *Phys. Rev. B* **58**, 12193 (1998).
- ⁷J. Zhang, Y. K. Takahashi, R. Gopalan, and K. Hono, *Appl. Phys. Lett.* **86**, 122509 (2005); A. J. Zambano, H. Oguchi, I. Takeuchi, Y. Choi, J. S. Jiang, J. P. Liu, S. E. Lofland, D. Josell, and L. A. Bendersky, *Phys. Rev. B* **75**, 144429 (2007); W. C. Lin, B. Y. Wang, T. Y. Chen, L. C. Lin, Y. W. Liao, W. Pan, N. Y. Jih, K. J. Song, and M. T. Lin, *Appl. Phys. Lett.* **90**, 052502 (2007); G. Asti, M. Ghidini, R. Pellicelli, C. Pernechele, M. Solzi, F. Albertini, F. Casoli, S. Fabbri, and L. Paretì, *Phys. Rev. B* **73**, 094406 (2006).
- ⁸Y. Choi, J. S. Jiang, Y. Ding, R. A. Rosenberg, J. E. Pearson, S. D. Bader, A. Zambano, M. Murakami, I. Takeuchi, Z. L. Wang, and J. P. Liu, *Phys. Rev. B* **75**, 104432 (2007).
- ⁹J. S. Jiang, J. E. Pearson, Z. Y. Liu, B. Kabius, S. Trasobares, D. J. Miller, S. D. Bader, D. R. Lee, D. Haskel, G. Srajer, and J. P. Liu, *Appl. Phys. Lett.* **85**, 5293 (2004).
- ¹⁰Y. Choi, J. S. Jiang, J. E. Pearson, S. D. Bader, and J. P. Liu, *Appl. Phys. Lett.* **91**, 072509 (2007).
- ¹¹J. Liu and J. M. Cowley, *Ultramicroscopy* **37**, 50 (1991); Z. L. Wang, *ibid.* **53**, 73 (1994).
- ¹²K. Buschow, *Acta Crystallogr., Sect. B: Struct. Crystallogr. Cryst. Chem.* **26**, 1389 (1970).
- ¹³J. R. Thomson, *J. Less-Common Met.* **10**, 432 (1966).
- ¹⁴Z. J. Guo, J. S. Jiang, J. E. Pearson, S. D. Bader, and J. P. Liu, *Appl. Phys. Lett.* **81**, 2029 (2002).